2nd International Conference on Experiments/Process/System Modelling/Simulation & Optimization
2nd IC-EpsMsO
Athens, 4-7 July, 2007

A NUMERICAL SIMULATION OF FLOW AND MIXED CONVECTION INSIDE VERTICAL ECCENTRIC ANNULUS

M.R.H. Nobari [1], Ali Asgarian [2]

[1] Associate Professor, E-mail: mrnobari@cic.aut.ac.ir
[2] Graduate Student, E-mail: asgarian@gmail.com

Amirkabir University of Technology, Mechanical Engineering Department, 424 Hafez Ave.,
P.O. Box 15875-4413, Tehran, Iran

Keywords: Numerical Simulation, Mixed Convection, Eccentric Annulus

Abstract. *In this article, mixed convection heat transfer is numerically studied in a vertical eccentric annulus. For this purpose, full Navier-Stokes equations along with energy equation are solved in a 3D orthogonal grid using bipolar cylindrical coordinate system and finite volume method based on SIMPLE algorithm .*
To investigate flow and heat transfer in the presence of gravity, the inner wall of the annulus is kept at a constant temperature, while the outer wall is assumed to be insulated. The effect of different governing non-dimensional parameters consisting of dimensionless eccentricity (E), radius ratio (N) and mixed convection parameter (Gr/Re) on the flow and temperature field are studied in detail. The numerical results obtained are in good agreement with previous numerical works.
Furthermore, the effect of internal longitudinal fins on the inner wall of the annulus on the flow field and heat transfer is carried out for the first time in this paper. The numerical results obtained in this case indicate uniform temperature field comparing the finless case. In addition, the amount of augmented heat transfer due to adding internal fins is discussed.

NOMENCLATURE

a	location of the positive pole of the bipolar coordinate system, $r_i \mathrm{Sinh}\eta_i$ or $r_o \mathrm{Sinh}\eta_o$
D_h	hydraulic diameter of annulus, $2(r_o - r_i) = 2a(1-N)Csch\eta_o$
e	eccentricity (distance between the two centers of the two cylinders forming the eccentric annulus), $a\ (Coth\eta_o - Coth\eta_i)$
E	dimensionless eccentricity $\frac{e}{r_o - r_i} = \frac{Coth\,\eta_o - Coth\,\eta_i}{Csch\,\eta_o - Csch\,\eta_i}$
g	gravity acceleration
Gr	Grashof number, $\frac{g\beta(T_w - T_o)D_h^3}{\upsilon^2}$
h	coordinate transformation scale factor, $a/(Cosh\eta - Cos\xi)$
k	thermal conductivity of fluid
H	dimensionless coordinate transformation factor, h/D_h
L	height of annulus
m	number of grids in ξ direction
n	number of grids in η direction
N	radius ratio, $\frac{r_i}{r_o} = \frac{Sinh\,\eta_o}{Sinh\,\eta_i}$
Nu	Nusselt number, $\frac{q'' D_h}{k(T_W - T_0)}$
$\overline{Nu}_i$	Nusselt number averaged around the periphery of the inner wall, $\frac{2(1-N)}{N\pi}\int_0^\pi Nu_i\, H(\eta_i,\xi)d\xi$
$\overline{\overline{Nu}}_i$	Nusselt number totally averaged circumferentially and axially along the inner wall, $\frac{1}{z}\int_0^z \overline{Nu}\, dz$
p	pressure
p_0	inlet pressure
p^*	dimensionless pressure, $\frac{p - p_o}{\rho\overline{w}^2}$
Pr	prandtl number, $\frac{\upsilon}{\alpha} = \frac{\mu c}{K}$
q	number of grids in z direction
r_i	radius of inner cylinder
r_o	radius of outer cylinder
Re	Reynolds number, $\frac{\rho\overline{w}D_h}{\mu}$
S	source term in conservation equations
T	temperature
T_b	bulk temperature, $\int_A TwdA/(A\overline{w}) = 2\int_0^\pi\int_{\eta_o}^{\eta_i} Twh^2 d\eta d\xi/[\pi(r_o^2 - r_i^2)\overline{w}]$
T_w	inner wall temperature

T_0	inlet temperature	z^*	dimensionless axial coordinte
u	velocity component in ξ direction,	***Greek symbols***	
u^*	dimensionless velocity component in ξ direction, $u/\overline{w}$	ξ	the first coordinate in bipolar system
		η	the second coordinate in bipolar system
v	velocity component in η direction	η_i	value of η on the inner surface of the annulus
v^*	dimensionless velocity component in η direction, $v/\overline{w}$	η_o	value of η on the outer surface of the annulus
		θ	dimensionless temperature, $\frac{T-T_0}{T_W-T_0}$
w	axial velocity	ρ	density
w^*	dimensionless axial velocity, $w/\overline{w}$	μ	dynamic viscosity
$\overline{w}$	average axial velocity, $\int_A wdA/A = 2\int_0^{\pi}\int_{\eta_o}^{\eta_i} wh^2 d\eta d\xi/[\pi(r_o^2-r_i^2)]$	υ	kinematic viscosity
		β	volumetric coefficient of thermal expansion
		Φ	general variable
x	the first coordinate in Cartesian system	Θ	normalized η, $\frac{\eta-\eta_0}{\eta_i-\eta_0}$
y	the second coordinate in Cartesian system		
z	axial coordinate, z/D_h		

1 INTRODUCTION

The problem of flow through a vertical eccentric annulus and its corresponding mixed convection heat transfer is usually encountered in many industrial applications. One to name is drilling operation in oil/gas wells. Eccentricity can also arise due to poor manufacturing process or bad installation procedure which is referred as nominal eccentricity. Other examples in which eccentricity problem is observed are double-pipe heat exchangers; nuclear reactors; vertical electrical motors; solar heating systems and power distribution cables' cooling. One common practice to increase heat transfer rate and to decrease the size of the heat exchangers is internal fins. Despite the increase in pump power demand to overcome the pressure drop, internal fins are considered for improvement of heat transfer features.

By considering the above lines it seems natural that there exists an excellent research literature on the subject. In an experimental-analytical work, Reynolds, Lundberg and McCuen [1] have suggested four principal Boundary conditions for convective heat transfer through the annulus (both concentric and eccentric) which formed a foundation for future researches. Feldman, Hornbeck and Osterle [2], [3] have investigated the developing of laminar flow and temperature field in eccentric annular ducts separately in two articles. Their solution was numerical and based on finite difference method. They used only two equations (continuity and axial momentum) to obtain the flow field. It is clear that the number of variables was more than equations but they considered the transverse pattern for secondary flow and completed their mathematical model with results of this hypothesis. Singh and Rajvanshi [4] presented the perturbation solution of heat transfer for eccentric cylinders rotating with different velocities. The solution has been obtained by using a bipolar coordinate system. EL-Shaarawi and El-Nimr's article [5] have treated of notable analytical solution for free convection heat transfer of developed flow in concentric vertical annulus. They obtained correlations for velocity and temperature fields, volumetric flow rate, average and overall Nusselt number. EL-Shaarawi, Abualhamayel and Mokheimer [6] have studied the developing forced convection in vertical eccentric annulus again, after Feldman et al. [2], [3]. They tried to solve the problem with less approximation, so presented a numerical algorithm based on finite difference method and implemented this algorithm in their next works. But their model had also simplifications based on boundary layer theory, which assumed that: the pressure is a function of the axial coordinate only, the axial diffusions of momentum and energy are neglected, and the radial-like velocity component is much smaller than the others. These assumptions resulted in dropping one of momentum equations (in η direction). For the first time mixed convection in the same geometry has studied by Mokheimer and El-Shaarawi [7]. They employed the bousinesque approximation to consider the buoyancy force and solved the equation with the same method as in [6]. Their results analyzed the developing of axial velocity profiles, variation of pressure through the length of duct and heat transfer parameters in details. In another article [8], they obtained the critical values of buoyancy parameter ($Gr/Re|_{Cr}$) for mixed convection in eccentric annulus with analytical solution. In this critical value the buoyancy force will be equal to friction resistance and no pressure drop will be seen. Mokheimer and Sami [9] in the case of first principle thermal boundary condition (both of walls were kept at constant temperatures) investigated the condition for pressure build-up due to buoyancy effects. De Pina and Carvalho [10] for oil/gas well drilling purpose solve the flow in annular Space with Axially Varying Eccentricity. They simplified the 3D Navier-Stokes equations into two 2D differential equations based on lubrication approximation. Ingham and Patel [11] presented an overview of developing combined convection of non-Newtonian fluids.

This article deals with flow and mixed convection in vertical eccentric annulus which its inner wall is kept at constant temperature (T_w) while the outer one is insulated. Here we use the full Navier-Stokes equations in 3D

form and try to minimize the approximations. The governing equations are discritized on an orthogonal structured grid in bipolar coordinate system. Implementation of finite volume method and SIMPLE algorithm to solve the equations is a new numerical approach that employed in this work. Furthermore, we study the effect of Adding longitudinal fins to the inner wall of channel on flow field and temperature.

2 GOVERNING EQUATIONS

Geometry of the annulus duct is illustrated in Fig. 2. Flow with uniform axial velocity (W_0) and ambient temperature (T_0) enters the bottom inlet of annulus. During the upward motion of the fluid, the flow becomes hydrodynamically and thermally fully developed. On the other hand, because of heat transfer from inner wall, the onset of free convection is observed.

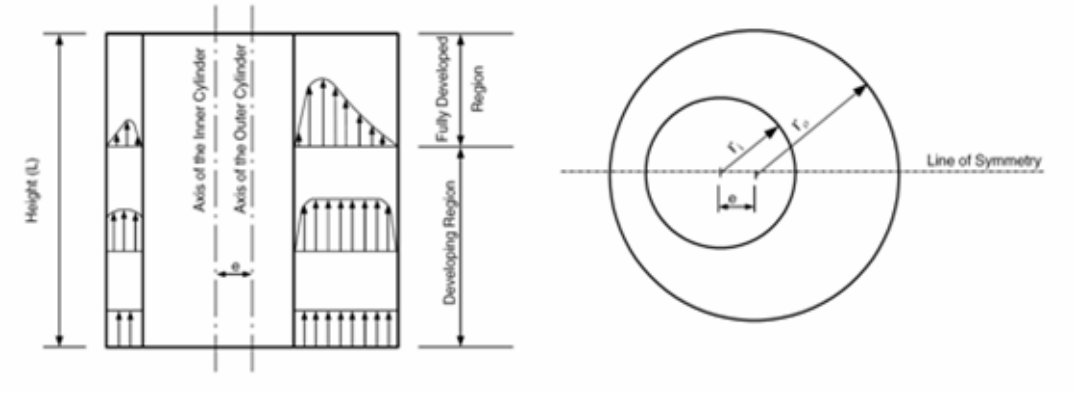

Figure 2. Geometry of the annulus duct

Governing equations including continuity, momentum and energy balances are written in bipolar cylindrical coordinate system. The coordinate is defined with three components (ξ, η, z) as shown in Fig. 3. The key features of this coordinate are that the generated grid will be orthogonal so the computational error associated with non-orthogonality of the cell faces will be reduced and the grid generation process will be simplified.

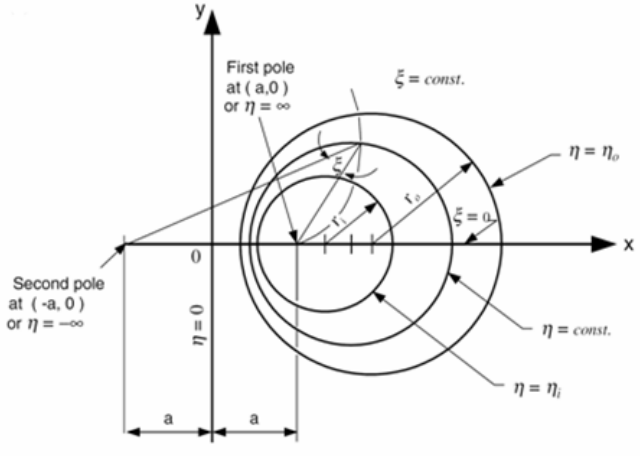

Figure 3. Bipolar coordinate system

The transformation equation between bipolar and Cartesian coordinate system is as follows,

$$\begin{cases} x = \dfrac{a\sinh(\eta)}{Cosh(\eta)-Cos(\xi)} \\ y = \dfrac{a\sin(\xi)}{Cosh(\eta)-Cos(\xi)} \\ z = z \end{cases} \tag{1}$$

The z-axis in cylindrical bipolar coordinate is aligned on Cartesian z-axis. ξ values is between 0 and 2π, while η changes over the range of -∞ to ∞. As illustrated in Fig. 3 the locus of the constant-η points is a set of circles,

center of which is located on the x-axis at the point (*acoth(η), 0*). Also the locus of constant-ξ points is circles with radius of *a /sin(ξ)* which are centered at the point (*0, acot(ξ)*) on the y-axis. Constant-η circles were utilized to generate eccentric cylinders. The values $\eta = \eta_i$ and $\eta = \eta_o$ represent respectively inner and outer cylinders. By considering the existing symmetry only a half-section of the annulus is needed as below,

$$0 \le \xi \le \pi \qquad \eta_o \le \eta \le \eta_i \qquad 0 \le z \le L \tag{2}$$

Now by reference to the vector form of the governing equations and making the use of vector operators in orthogonal curvilinear coordinate system [12], [13] and [14] equations are written in bipolar system.

Basic assumptions made are as following: The fluid is assumed to be Newtonian, incompressible (density changes are only included in buoyancy term) and the physical properties were taken constant. Also the body forces are taken zero in all directions but axial (buoyancy). Radiation and viscous dissipation is neglected and there is no internal energy production too.

In order to consider the buoyancy force in axial momentum equation, Bousinesque approximation is implemented and the body force in z-direction is considered as $\rho g\beta(T-T_0)$. Since the numerical scheme is finite volume, it is needed to write the conservative form of the equations[1]. Therefore we add the zero value term ($\phi \nabla . V$) to the LHS of non-conservative equations to produce the term $\nabla.(\phi V)$, while the extra terms are included in source term on the RHS. After non-dimensionalization we get,

Continuity

$$\frac{1}{H^2}\left[\frac{\partial}{\partial\xi}(Hu^*)+\frac{\partial}{\partial\eta}(Hv^*)+H^2\frac{\partial w^*}{\partial z^*}\right]=0 \tag{3}$$

ξ-momentum equation

$$\frac{1}{H^2}\left[\frac{\partial}{\partial\xi}(Hu^{*2})+\frac{\partial}{\partial\eta}(Hu^*v^*)+H^2\frac{\partial}{\partial z^*}(u^*w^*)\right]=\frac{1}{\mathrm{Re}}\frac{1}{H^2}\left[\frac{\partial^2u^*}{\partial\xi^2}+\frac{\partial^2u^*}{\partial\eta^2}+H^2\frac{\partial^2u^*}{\partial z^{*2}}\right]+S_\xi^* \tag{4}$$

η-momentum equation

$$\frac{1}{H^2}\left[\frac{\partial}{\partial\xi}(Hu^*v^*)+\frac{\partial}{\partial\eta}(Hv^{*2})+H^2\frac{\partial}{\partial z^*}(v^*w^*)\right]=\frac{1}{\mathrm{Re}}\frac{1}{H^2}\left[\frac{\partial^2v^*}{\partial\xi^2}+\frac{\partial^2v^*}{\partial\eta^2}+H^2\frac{\partial^2v^*}{\partial z^{*2}}\right]+S_\eta^* \tag{5}$$

z-momentum equation

$$\frac{1}{H^2}\left[\frac{\partial}{\partial\xi}(Hu^*w^*)+\frac{\partial}{\partial\eta}(Hv^*w^*)+H^2\frac{\partial}{\partial z^*}(w^{*2})\right]=\frac{1}{\mathrm{Re}}\frac{1}{H^2}\left[\frac{\partial^2w^*}{\partial\xi^2}+\frac{\partial^2w^*}{\partial\eta^2}+H^2\frac{\partial^2w^*}{\partial z^{*2}}\right]+S_z^* \tag{6}$$

Energy equation

$$\frac{1}{H^2}\left[\frac{\partial}{\partial\xi}(Hu^*\theta)+\frac{\partial}{\partial\eta}(Hv^*\theta)+H^2\frac{\partial}{\partial z^*}(w^*\theta)\right]=\frac{1}{\mathrm{Re}\,\mathrm{Pr}}\frac{1}{H^2}\left[\frac{\partial^2\theta}{\partial\xi^2}+\frac{\partial^2\theta}{\partial\eta^2}+H^2\frac{\partial^2\theta}{\partial z^{*2}}\right] \tag{7}$$

Where

$$S_\xi^*=\frac{v^{*2}}{H^2}\frac{\partial H}{\partial\xi}-\frac{u^*v^*}{H^2}\frac{\partial H}{\partial\eta}+\frac{1}{\mathrm{Re}}\left[-\frac{2}{H^3}\frac{\partial H}{\partial\xi}\frac{\partial v^*}{\partial\eta}+\frac{2}{H^3}\frac{\partial H}{\partial\eta}\frac{\partial v^*}{\partial\xi}-\frac{2}{H^4}\left(\frac{\partial H}{\partial\eta}\right)^2u^*+\frac{1}{H^3}\frac{\partial^2H}{\partial\eta^2}u^*-\frac{2}{H^4}\left(\frac{\partial H}{\partial\xi}\right)^2u^*+\frac{1}{H^3}\frac{\partial^2H}{\partial\xi^2}u^*\right]-\frac{1}{H}\frac{\partial p^*}{\partial\xi} \tag{8}$$

[1] Conservation Equation : $\rho\frac{\partial\phi}{\partial t}+\rho\nabla.(\phi V)=\mu\nabla^2\phi+S$

$$S_\eta^* = \frac{u^{*2}}{H^2}\frac{\partial H}{\partial \eta} - \frac{u^* v^*}{H^2}\frac{\partial H}{\partial \xi} + \frac{1}{\mathrm{Re}}\left[-\frac{2}{H^3}\frac{\partial H}{\partial \eta}\frac{\partial u^*}{\partial \xi} + \frac{2}{H^3}\frac{\partial H}{\partial \xi}\frac{\partial u^*}{\partial \eta} - \frac{2}{H^4}\left(\frac{\partial H}{\partial \xi}\right)^2 v^* + \frac{1}{H^3}\frac{\partial^2 H}{\partial \xi^2} v^* - \frac{2}{H^4}\left(\frac{\partial H}{\partial \eta}\right)^2 v^* + \frac{1}{H^3}\frac{\partial^2 H}{\partial \eta^2} v^* \right] - \frac{1}{H}\frac{\partial p^*}{\partial \eta} \tag{9}$$

$$S_z^* = \frac{Gr}{\mathrm{Re}^2}\theta - \frac{\partial p^*}{\partial z^*} \tag{10}$$

Note that the pressure gradients are included at the end of source terms (8, 9, 10) to convert the equation into the conservation form, but for numerical solution (finite volume method) they should be appear in the main equations(4, 5, 6). The above equations are considered with the following boundary conditions.

-inlet ($z = 0$): $u^* = v^* = \theta^* = 0$, $w^* = 1$

-outlet ($z = L$): It is assumed that the flow becomes both hydrodynamically and thermally fully developed.

$$\frac{\partial u^*}{\partial z^*} = \frac{\partial v^*}{\partial z^*} = \frac{\partial w^*}{\partial z^*} = \frac{\partial \theta^*}{\partial z^*} = 0$$

To maintain the validity of this assumption, the duct length is considered large enough ($L=100D_h$).

-Inner wall ($\eta = \eta_i$): By considering the no-slip condition and associated thermal condition we can write,

$$u^* = v^* = w^* = 0 \ , \ \theta = 1$$

-outer wall ($\eta = \eta_o$):

$$u^* = v^* = w^* = 0 \ , \ \frac{\partial \theta}{\partial \eta} = 0$$

-Primary ($\xi=0$) and secondary ($\xi=\pi$) symmetry planes: Since there's no cross flow through the symmetry boundary the corresponding velocity component perpendicular to this boundary is set zero. For other quantities the derivative in normal direction is negligible.

$$u^* = 0 \ , \ \frac{\partial v^*}{\partial \xi} = \frac{\partial w^*}{\partial \xi} = \frac{\partial \theta}{\partial \xi} = 0$$

3 NUMERICAL METHOD

Finite volume method (SIMPLE algorithm) is used to solve the equations. We claim that this is the first time for this problem being solved with F.V. method. Using the bipolar coordinate system facilitates the generation of a structured and orthogonal grid. An easy method to generate the grid is to divide all intervals into equal segments. If m, n, and q represent number of segments in ξ, η and z directions respectively, one can write,

$$\Delta\xi = \frac{\pi}{m} \ , \ \Delta\eta = \frac{\eta_i - \eta_0}{n} \ , \ \Delta z = \frac{L}{q} \tag{11}$$

In this manner a uniform computational grid is obtained. But because of interdependency between dimensions of physical grid and scale factor (h) which is itself function of ξ and η, obtained physical grid will be highly non-uniform which in turn increases errors in interpolations and cell's surface and volume computations. To obtain a uniform physical grid we have to change interval divisions. In other words $\Delta\xi$ and $\Delta\eta$ are no longer constant and vary in a way that physical dimensions of the grid $h(\xi,\eta)\Delta\xi$ and $h(\xi,\eta)\Delta\eta$ remain almost constant. However because of the eccentricity a fully uniform grid can never be met.

To calculate $\Delta\xi$ and $\Delta\eta$ at different locations of domain two non-linear equations are solved numerically. But divisions in z-direction are considered uniform ($\Delta z=L/q$).

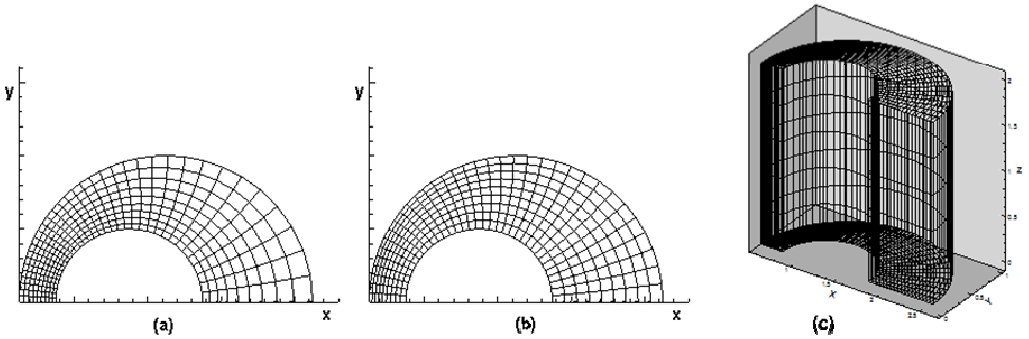

Figure 4. (a) Section of Non-uniform grid (b) Section of uniform grid (c) 3D grid

Most of the runs are for the case in which divisions in ξ, η and z directions are $m = 60$, $n = 18$ and $q = 250$ respectively. In order to check the grid independency of the code, the results for three different grids have been compared to each other which show a good agreement.

Because of the zigzag treatment of pressure, Staggered grid is used to discritize the equations. The value of the variables and associated derivatives are calculated with power-law scheme. Since the source terms in ξ and η momentum equations are functions of dependent variable, we have to linearize them with existing methods [16]. To solve the equations SIMPLE algorithm is implemented. Energy equation should be solved simultaneously with momentum equations, since the buoyancy term ($\theta.Gr/Re^2$) in z component of momentum equation depends on temperature. In order to maintain a stable solution SOR method is used with under-relaxation factors equal to *0.7*. In all cases of running the code, after converging, maximum value obtained for residuals is of *O(10-6)*.

3 RESULTS AND DISCUSION

The results obtained from the code can be divided into two categories. The first is related to finless duct and the second case is the duct with internal fins. In the latter case it is assumed that six longitudinal fins are installed on the inner wall such that the angle between fins is 60° and the height of each fin is equal to one-half of the annulus width at the same location. The thickness of the fins is negligible and the whole height of the fin has the same temperature as its base, i.e. inner wall.

Since the main goal of the present paper is to analyze the effect of different governing non-dimensional parameters, the computer code is run for following cases.

Geometrical parameters: $N = 0.3, 0.5, 0.7, 0.9$ and $E = 0.1, 0.3, 0.5, 0.7$

Physical parameters: $Pr = 0.7$, $Re = 100$ and $Gr/Re = 0, 50, 100, 200, 250$

In fact the non-dimensional number seen in the governing equations is Richardson number which is defined as $Ri = Gr/Re^2$. But since in literature the ratio Gr/Re is chosen as the mixed convection parameter, we have done the same too.

In order to verify the obtained results from the code, they are compared with the latest and most similar research done by Mokheimer and El-Shaarawi [7]. As stated in the introduction, they have made more simplifying assumptions than what we have made here. As it can be seen in Fig. 5, in all the cases compared maximum difference between two sets of results is less than *5%*.

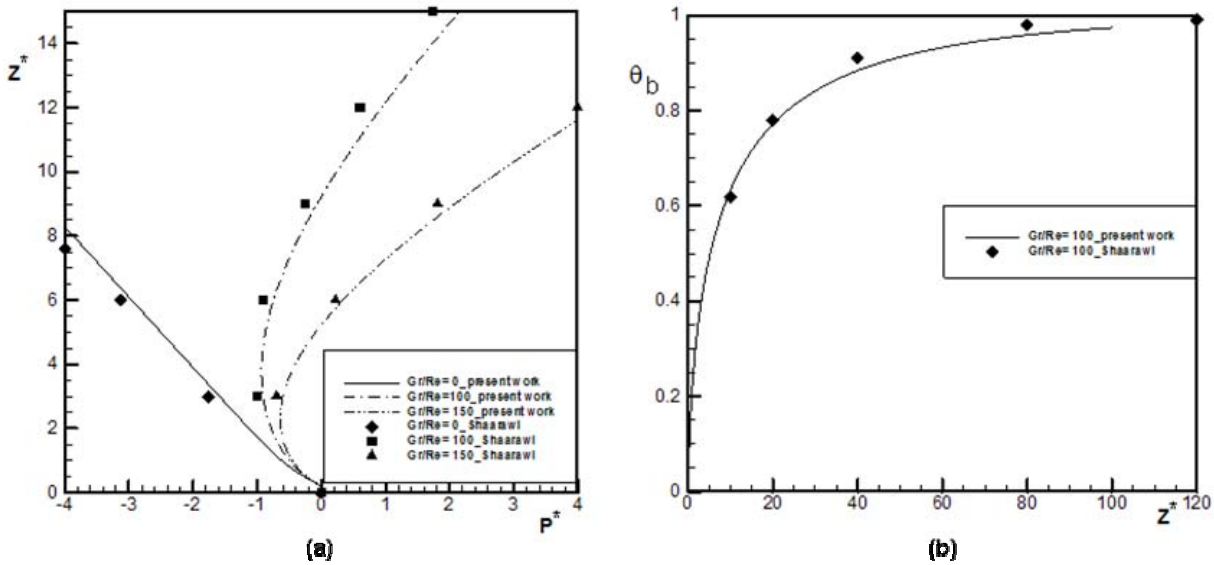

Figure 5. Comparison between present work and El-Shaarawi's results (a) Variation of pressure in axial direction (N=0.9 and E=0.1) (b) Variation of bulk temperature in axial direction (N=0.9 and E=0.7)

3.1 Finless duct

Fig. 6 shows the development of axial velocity in three different sections of the duct. The flow is uniform at inlet but because of eccentricity the resistance upon the flow is stronger in narrow region of cross section compared to the wider region. Then it can be seen that after the profile 2, the axial velocity in narrow region decays while in wide region it has an increasing trend. For high values of Gr/Re or E the flow reversal is

observed in narrow region (it is the case after the profile 10), but in intermediate area (b) the process happens slowly and smoothly.

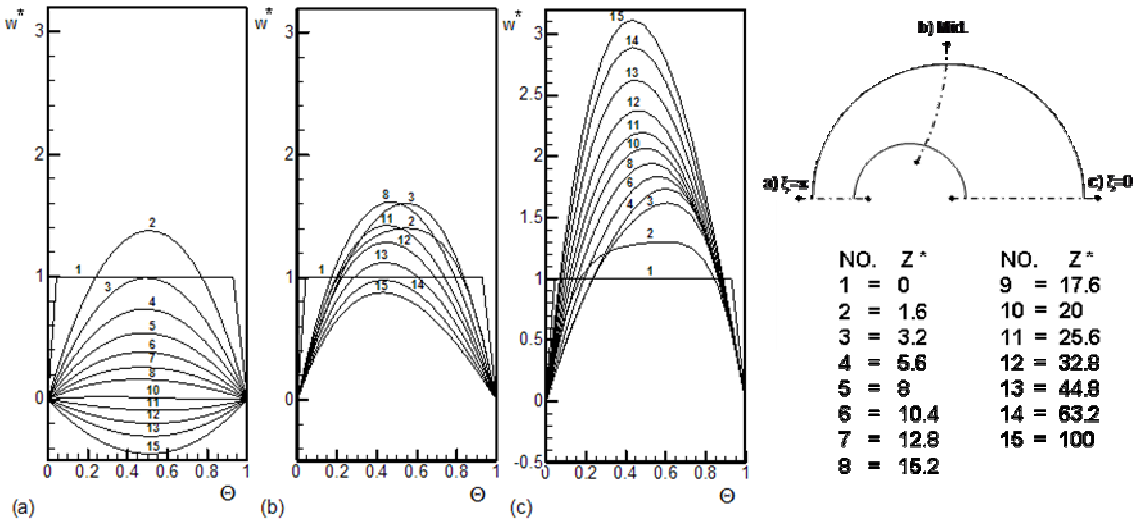

Figure 6. Development of the axial velocity profiles at N=0.7, E=0.3, Gr/Re=100
(a) narrow region (b) middle region (c) wide region
$\Theta = (\eta - \eta_o)/(\eta_i - \eta_o)$ Outer wall ($\Theta = 0$) inner wall($\Theta = 1$)

To better understand the behavior of axial velocity, its distribution in different cross sections has been represented in Fig. 7(a). This figure shows that the axial velocity's peak shifts toward the inner wall and that is because of higher temperature of this wall. But as the flow moves downstream and reaches to a fully-developed profile this peak point comes back to the middle of the gap.

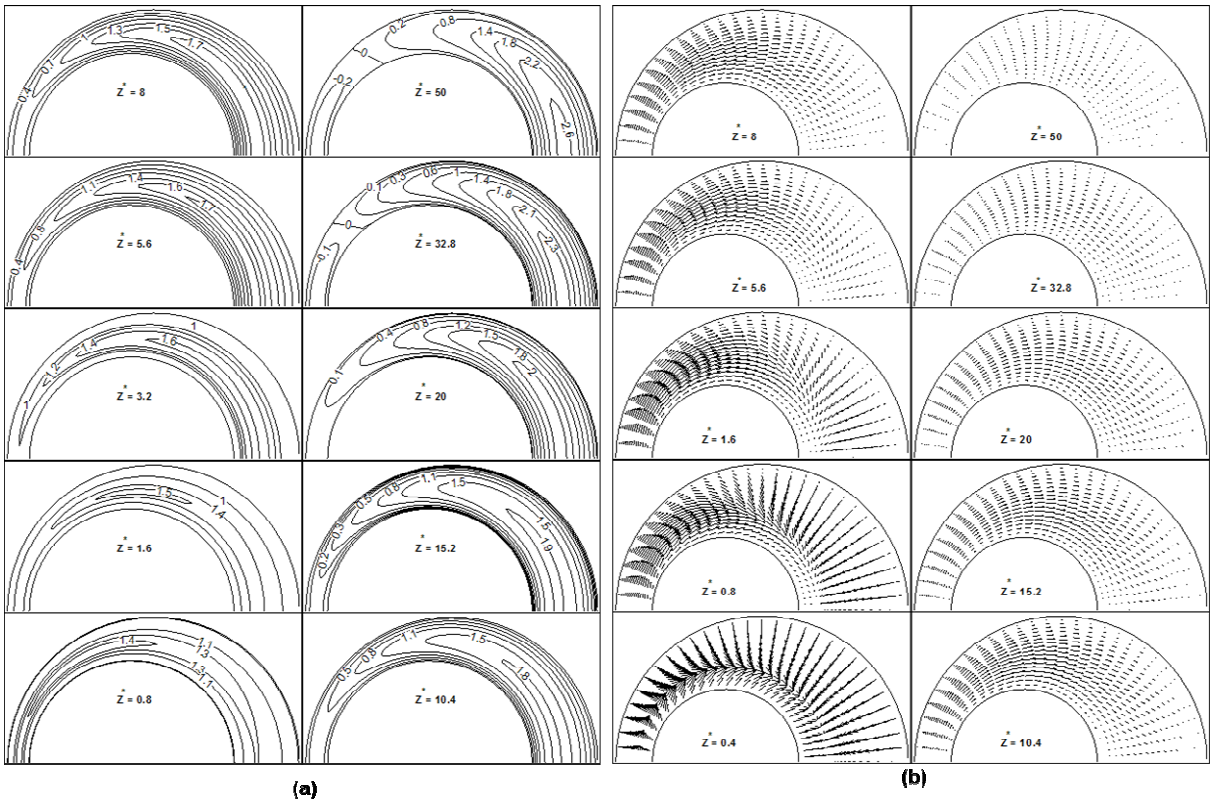

Figure 7. (a) Contours of the axial velocity at N=0.7 (b) Secondary flow vectors at N=0.5
both at E=0.5, Gr/Re=100

In previous investigations secondary flows have not been addressed well, but in this work since we have obtained a fully three dimensional solution, the pattern of these flows is studied perfectly. In Fig. 7(b) it can be

seen that near the inlet ($z^* = 0.4$) secondary flow begins to form and the direction of this flow is generally from narrow region to wider regions. This explains the growth of axial velocity in wide region. The secondary flow at $z^* = 0.4$ reminds us of the transverse flow hypothesis of Feldman et. al [2]. But this figure shows that this phenomenon happens just near the inlet and far more downstream the hypothesis is no longer valid. Furthermore by increasing z^* and approaching the hydrodynamic fully developing, secondary flow gradually decays in magnitude and finally diminishes completely at fully developed length.

From a practical engineer's point of view pressure losses are far more important than the precise shape of the velocity profile. In figures 8(a) and 8(b), minus signed pressure gradient ($-dp^*/dz^*$) has been plotted for various values of *Gr/Re* and E. As it can be seen from Fig. 8(a), for the case of forced convection (*Gr/Re=0*) the plot begins with a large value at inlet and decays rapidly and after that stays at a constant value. The point of reaching this constant value is in fact the location of fully developed length. This trend is the same for other *Gr/Re* values. However an increase in *Gr/Re* delays the fully developing and decreases the final value of pressure drop (at fully developed length) such that for *Gr/Re > 40* it leads to negative values of pressure drop. This means that increasing *Gr/Re* leads to the increased participation of buoyancy forces such that it can finally dominate the frictional resistance. This diffuser-like behavior can be interesting to designers, since they can decrease power demand of the pump. As illustrated in Fig. 8(b) at higher values of eccentricity pressure drop decreases.

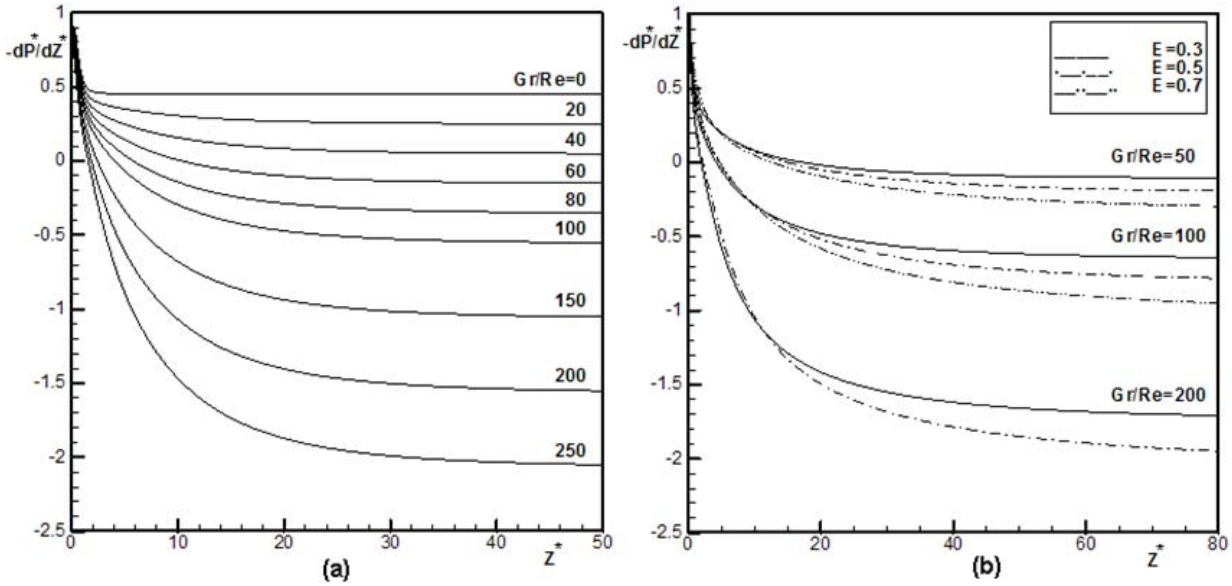

Figure 8. Variation of pressure loss in axial direction for different
(a) values of Gr/Re at N=0.7, E=0.1(b) eccentricities at N=0.7

To analyze temperature developing along the duct, we use mixed average temperature (bulk temperature). In Fig. 9(a) it has been plotted for different values of eccentricity. Decreasing the eccentricity leads to increased values of average temperature and accelerated trend of fully developing. Also in Fig. 9(b) temperature distribution in different cross sections of the duct is shown.

For study the effect of different parameters on heat transfer, overall Nusselt number is drawn against these parameters. Fig 9(c), 10(a) and 10(b) show that overall Nussel number increases as the eccentricity and radius ratio decrease and Gr/Re increases

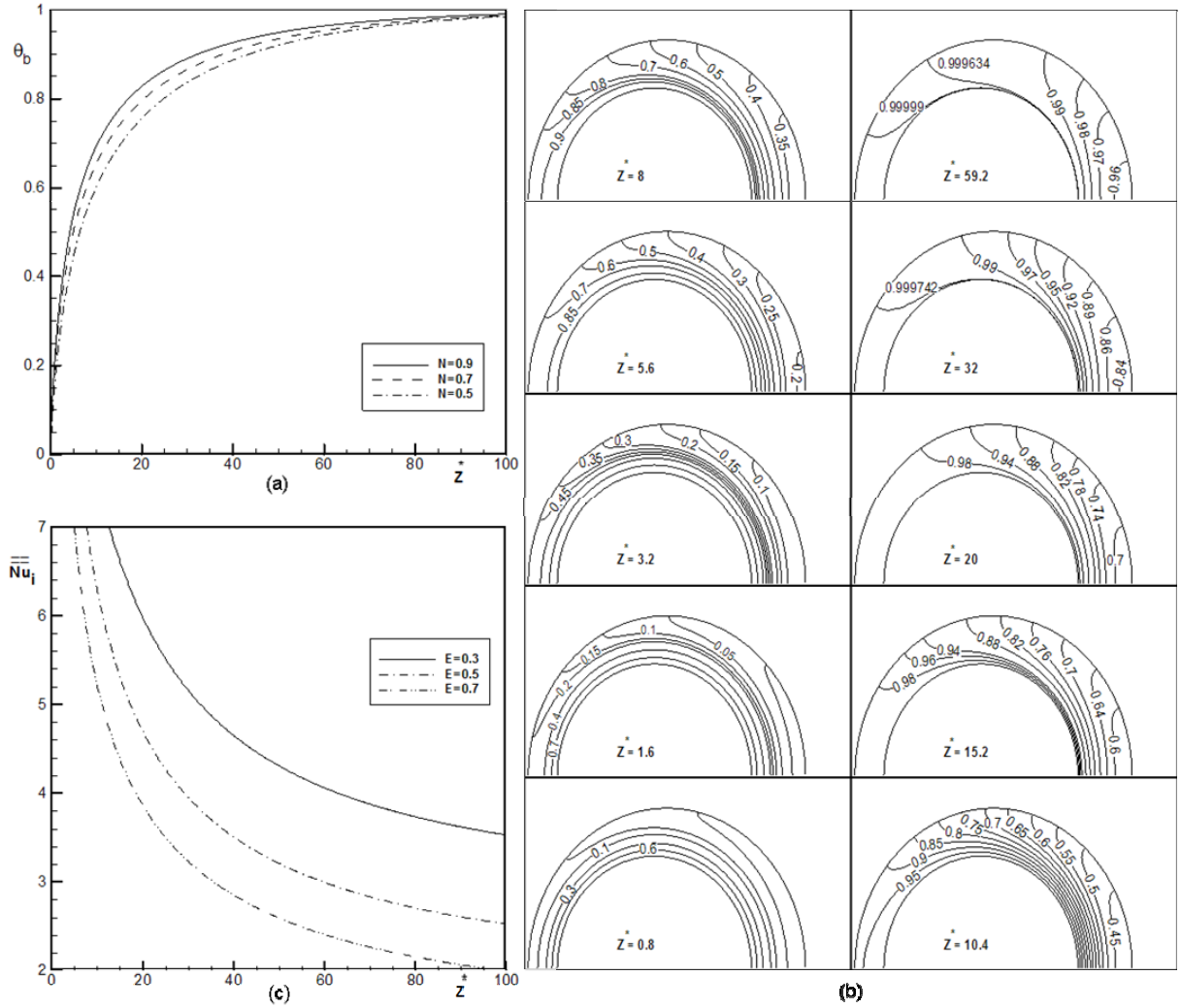

Figure 9.(a) Variation of Bulk temperature in the axial direction for different values of N at E=0.5, Gr/Re=100 (b) Contours of temperature at N=0.7, E=0.3, Gr/Re=100 (c) Variation of overall Nusselt number in the axial direction for different value of E at N=0.7, Gr/Re=100

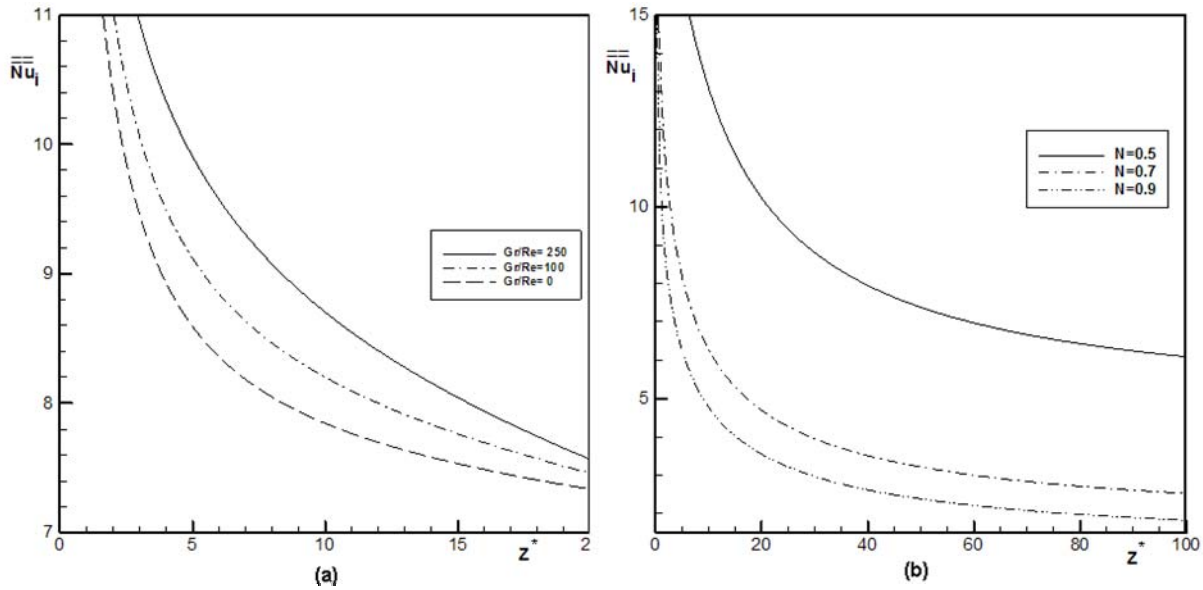

Figure 10. Variation of overall Nusselt number in the axial direction for different values of (a) Gr/Re at N=0.7, E=0.1(b) N at E=0.5, Gr/Re=100

3.2 Duct with internal fins

There are many ways to increase heat transfer rate in internal flows. This can be done either by increasing convection coefficient or increasing the heat transfer surface. The later one can be gained with adding longitudinal fins inside the duct. Although it can be done, but we should care for pressure drop and associated increased power demand for pumping. In this section a thorough evaluation of these parameters will be presented along with a comparison to the finless case.

For the case of finned duct, axial velocity developing has been investigated in three axial sections ($\alpha = \pi/6\ ,\ \pi/2,\ 5\pi/6$). Fig. 11 suggests an overall similarity between axial velocity's profiles with that of finless duct

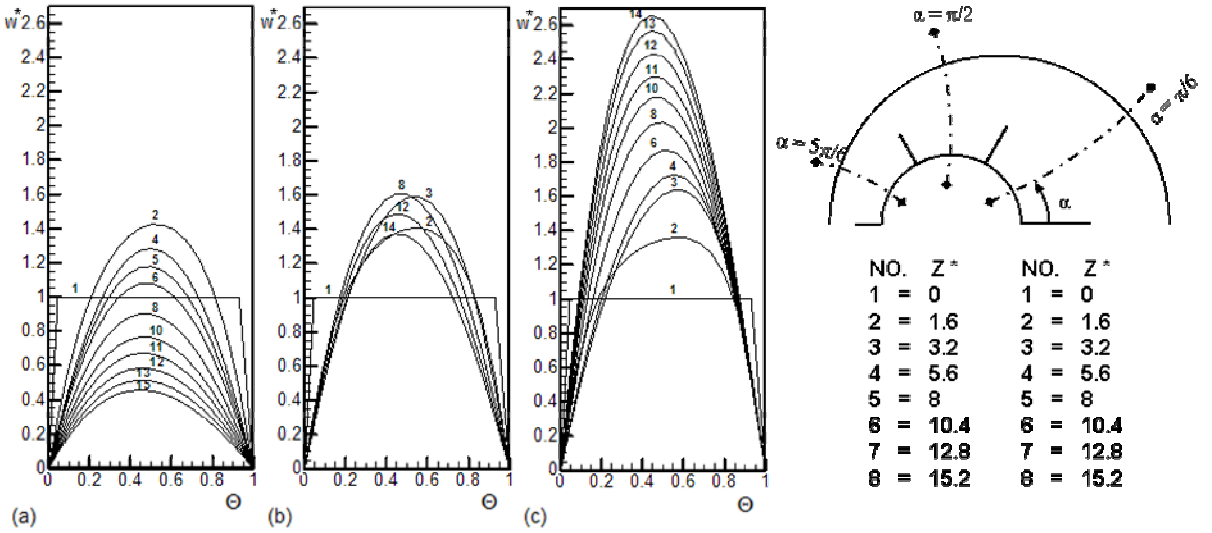

Figure 11. Development of the axial velocity profiles in finned duct at N=0.7, E=0.3, Gr/Re=100
(a) narrow region (b) middle region (c) wide region
$\Theta = (\eta - \eta_o)/(\eta_i - \eta_o)$ Outer wall ($\Theta = 0$) inner wall($\Theta = 1$)

. Fig. 12(a) which shows axial velocity contours in cross sections of the duct is of more details. It can be seen that for the existence of the fins, velocity shell in every section has three tips instead of one single tip (counted just in the half-annulus under study). The fins are also an obstacle in the way of secondary flow formation. This moderates the decrease in axial velocity in narrow region such that because of fins there's no flow reversal in narrow region. On the other hand, by considering sections $z^* = 32.8$ and $z^* = 50$ it is observed that maximum axial velocity has increased compared to un-finned case. The reason lies in formation of boundary layer near the fins. The gradual thickening of this layer in streamwise direction makes the central core more compact and according to the continuity this indicates the increase in axial velocity in this region.

The presence of fins has a direct effect on the secondary flow. Number one, they are an obstacle in the way of secondary flow and partly reduce the size of the velocity vectors of secondary flow. Number two, near the fins the flow pattern changes due to reduction of cross section's width. These changes can be well viewed in Fig. 12(b). In section $z = 0.8$ near the inlet it is seen that with formation of boundary layer on the walls, the quasi-radial velocity component (v) is appreciable but by increasing of z it becomes negligible and the other component (u) increases as a result of eccentricity.

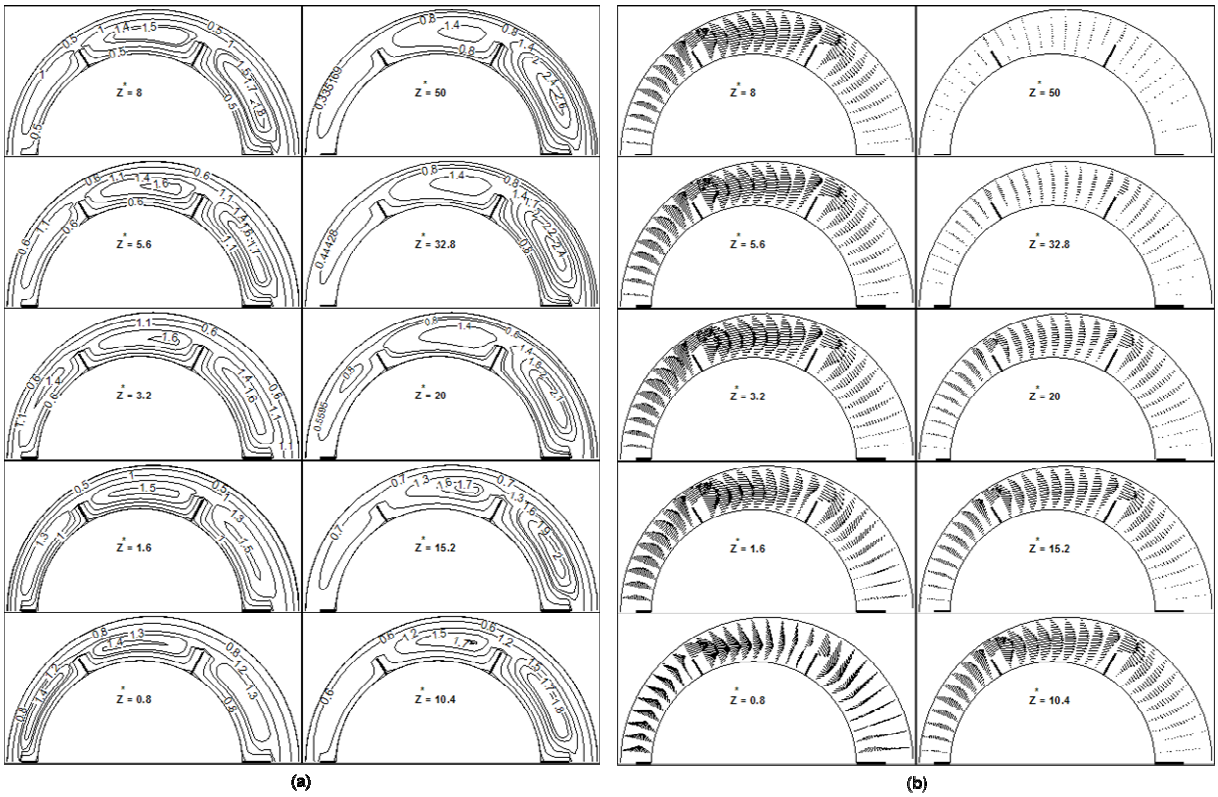

Figure 12. (a) Contours of the axial velocity (b) Secondary flow vectors
both in finned duct with N=0.7, E=0.5 at Gr/Re=100

In Fig. 13(a) a comparison has been made for pressure drop along the duct with and without fins at different values of *Gr/Re*. It can be seen in all cases pressure drop in finned duct is higher than duct without fin. The difference is a fixed (approximately 0.1) value. Such figures help us decide if the pressure drop due to fins is justifiable in comparison with the gain in heat transfer rate.

Fig 13(b) suggests that the comparison between the mixed average temperature for finned and un-finned ducts leads to conclusion that for the finned case average temperature has clearly increased and thermal developing has been accelerated. This means increased heat transfer. Also from Fig. 13(c) (in comparison with Fig. 9(b)) it is evident that fins have undeniable effect in increasing the heat diffusion in fluid and a more uniform temperature distribution within the cross section.

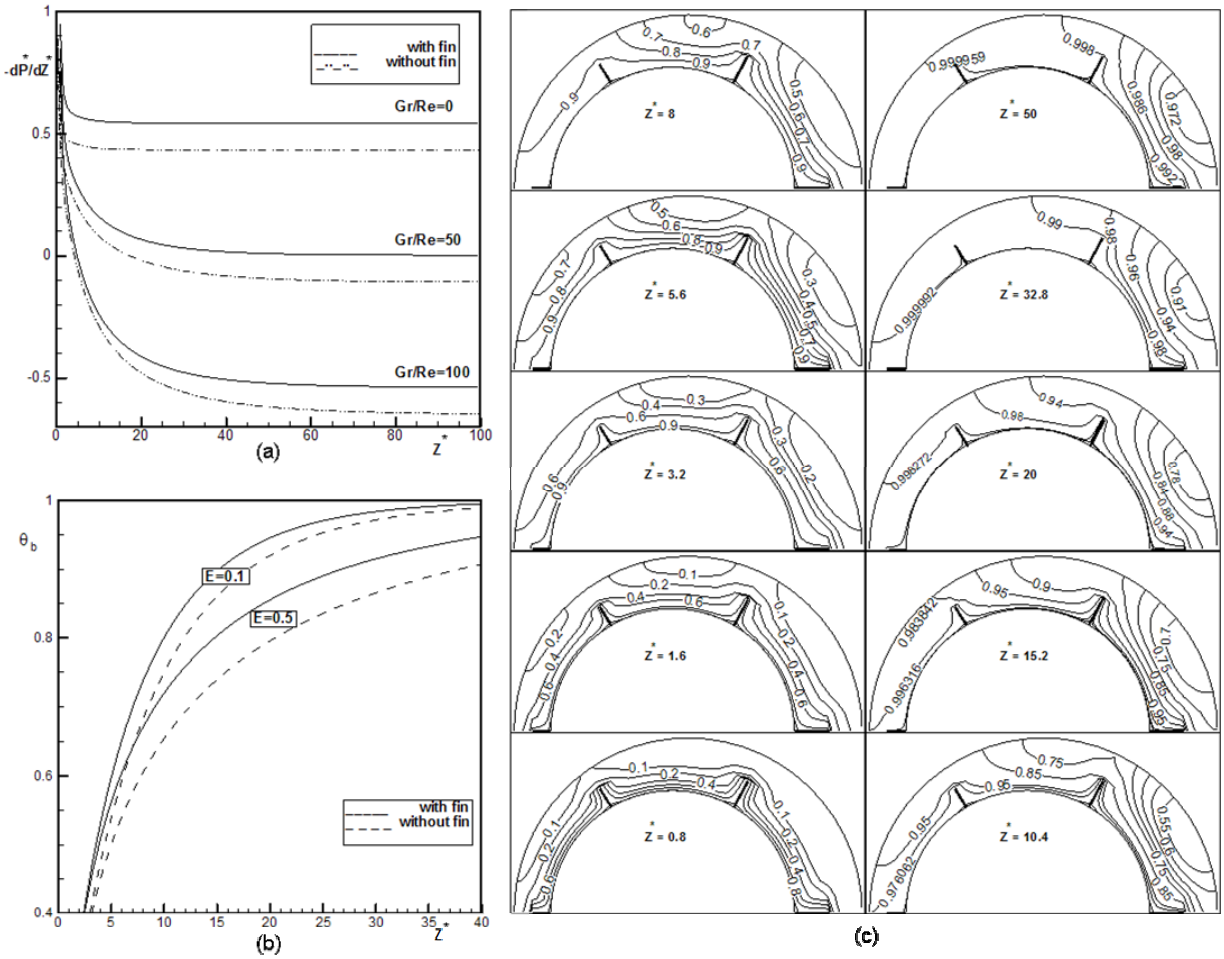

Figure 13.(a) Comparison of pressure loss between fined and finless ducts for different Gr/Re at N=0.7, E=0.3
(b) Comparison of bulk temperature between fined and finless ducts for different E at N=0.7, Gr/Re=100
(c) Isothermal contours in different sections of duct with N=0.7, E=0.3 at Gr/Re=100

REFERENCES

[1] Reynolds, W.C.; Lundberg, R.E.; McCuen P.A. " Heat Transfer in Annular Passages. General Formulation of the Problem for Arbitrarily Prescribed Wall Temperatures or Heat Fluxes. ". ***Int. J. Heat Mass Tran.*** 1963, Vol. 6, PP. 483-493

[2] Feldman, E.E.; Hornbeck, R.W.; Osterle, J.F. " A Numerical Solution of Laminar Developing Flow in Eccentric Annular Ducts ". ***Int. J. Heat Mass Tran.*** 1982, Vol. 25, No. 2, PP. 231-241

[3] Feldman, E.E.; Hornbeck, R.W.; Osterle, J.F. " A Numerical Solution of Developing Temperature For Laminar Developing Flow in Eccentric Annular Ducts ". ***Int. J. Heat Mass Tran.*** 1982, Vol. 25, No. 2, PP. 243-253

[4] Singh, Mohan; Rajvanshi, S.C. " Heat Transfer Between Rotating Eccentric Cylinders With Different Radii ". ***Int. J. Heat Mass Tran.*** 1982, Vol. 25, No. 11, PP. 1719-1724

[5] El-Shaarawi, M.A.I.; El-Nimr, M.A. " Fully Developed Laminar Natural Convection in Open-Ended Vertical Concentric Annuli ". ***Int. J. Heat Mass Tran.*** 1990, Vol. 33, No. 9, PP. 1873-1884

[6] El-Shaarawi, M.A.I.; Abualhamayel, H.I.; Mokheimer E.M.A. " Developing Laminar Forced Convection in Eccentric Annuli ". ***Heat Mass Tran.*** 1998, PP. 353-362

[7] Mokheimer, Esmail M.A.; El-Shaarawi, Maged .A.I. " Developing Mixed Convection in Vertical Eccentric Annuli ". ***Heat Mass Tran.*** 2004, Vol. 41, PP. 176-187

[8] Mokheimer, Esmail M.A.; El-Shaarawi, Maged .A.I. " Critical Values of Gr/Re for Mixed Convection in Vertical Eccentric Annuli with Isothermal/Adiabatic Walls ". ***J. Heat Tran.*** 2004, Vol. 126, PP. 479-482

[9] Mokheimer, Esmail M.A.; Sami S. " Condition for Pressure Build-Up Due to Buoyancy Effects on Forced Convection in Vertical Eccentric Annuli Under Thermal Boundary Condition of First Kind ". ***Heat Mass Tran.*** 2006, Vol. 43, PP. 175-189

[10] De Pina, Eduarda P.F.; Carvalho, M.S. " Three-Dimensional Flow of a Newtonian Liquid Through an Annular Space with Axially Varying Eccentricity ". ***J. Fluids Eng.*** 2006, Vol. 128, PP. 223-231

[11] Ingham, D.B.; Patel, N. " Developing Combined Convection of Non-Newtonian Fluids in an Eccentric Annulus ". ***Acta Mechanica*** 1997, Vol. 121, PP. 35-49

[12] Yuan, S.W., **Foundations of Fluid Mechanics**, New Jersey: Prentice-Hall Inc., 1967

[13] Hughes, W.F.; Gaylords, E.W., **Basic Equations of Engineering Science**, New York: Schaum., 1964

[14] Aris, R., **Vectors, Tensors, and the Basic Equations of Fluid Mechanics**, Englewood Cliffs, N.J.: Prentice-Hall, Inc., 1962

[15] Karamcheti, Krishnamurti, **Vector Analysis & Cartesian Tensors: with Selected Applications**, 1967

[16] Patankar, Suhaz V., **Numerical Heat Transfer and Fluid Flow**, New York: McGraw-Hill, 1980

[17] Ferziger, J.H.; Peric, M., **Coputational Method for Fluid Dynamics**, 3rd Ed., Berlin; New York; London: Springer, 2002

[18] Incropera, Frank P.; De Witt, David P., **Introduction to Heat Transfer**, Vol 1, 3rd Ed., USA: John Wiley & Sons Inc., 1996

[19] Kays, W.M.; Crawford, M.E., **Convective Heat and Mass Transfer**, New York: McGraw-Hill, 1978

[20] Bejan, Adrian, **Convection Heat Transfer**, New York: John Wiley & Sons Inc., 1984